Influence of the First Coordination of Uranyl on Its Luminescence Properties: A Study of Uranyl Binitrate with *N,N*-Dialkyl Amide DEHiBA and Water

Hanna Oher,[*,†,‡] Geoffroy Ferru,[¶] Laurent Couston,[¶] Laurence Berthon,[¶] Dominique Guillaumont,[¶] Florent Réal,[‡] Thomas Vercouter,[†] and Valérie Vallet[*,‡]

†*Université Paris-Saclay, CEA, Service d'Études Analytiques et de Réactivité des Surfaces (SEARS), F-91191 Gif-sur-Yvette CEDEX, France*

‡*Université de Lille, CNRS, UMR 8523 - PhLAM - Physique des Lasers Atomes et Molécules, F-59000 Lille, France*

¶*CEA, DES, ISEC, DMRC, Université de Montpellier, Marcoule, F-30207 Bagnols-sur-Ceze, France*

E-mail: hannaoher@gmail.com; valerie.vallet@univ-lille.fr

Abstract

Uranyl binitrate complexes have a particular interest in the nuclear industry, especially in the reprocessing of spent nuclear fuel. The modified PUREX extraction process is designed to extract U(VI) in the form of $UO_2(NO_3)_2(L)_2$ as has been confirmed by extended X-ray absorption fine structure (EXAFS), X-ray diffraction (XRD), and time-resolved laser-

induced fluorescence spectroscopy (TRLFS) measurements. In this study, the L ligands are two molecules of *N,N*-di-(ethyl-2-hexyl)isobutyramide (DEHiBA) monoamide used to bind uranyl in its first coordination sphere. DEHiBA ligands can coordinate uranyl in either *trans*- or *cis*-position with respect to the nitrate ligands, and these two conformers may coexist in solution. To use luminescence spectroscopy as a speciation technique, it is important to determine whether or not these conformers can be discriminated by their spectroscopic properties. To answer this question, the spectra of *trans*- and *cis*-$UO_2(NO_3)_2(DEiBA)_2$ conformers were modeled with *ab initio* methods and compared to the experimental time-resolved luminescence spectra on $UO_2(NO_3)_2(DEHiBA)_2$ systems. Moreover, the hydrated uranyl binitrate $UO_2(NO_3)_2(H_2O)_2$ complexes in the same *trans* and *cis* configurations were modeled to quantify the impact of organic DEHiBA on the luminescence properties.

Introduction

The production of electricity from nuclear energy has been developed in several countries. Some countries including the United States, France, and the United Kingdom chose to reprocess the spent nuclear fuel for an economic reuse of uranium and plutonium and a reduction of the radioactivity and volume of the wastes.[1] The recovery of uranium and plutonium and the effective separation from fission products and minor actinides has been achieved at both laboratory and industrial scales by solvent extraction techniques using an aqueous phase and an immiscible organic phase. The transfer of actinide metal cations occurs from an acidic aqueous phase resulting from the dissolution of the fuel in nitric acid into an organic phase by complexation with liposoluble extracting molecules.[2] Nowadays, the main industrial solvent extraction process is Plutonium Uranium Refining by Extraction (PUREX), in which the tri-*n*-butyl phosphate (TBP) extracting agent is used to separate U(VI) and Pu(IV) from minor actinides and fission products in highly concentrated nitric acid solution.[3] Although efficient, the PUREX process requires a reduction of plutonium for

the U/Pu partitioning by the addition of U(IV) and antinitrous reagents. Moreover, washing and recycling of the solvent have to account for the degradation of TBP by radiolysis.[4] Thus, several processes have been developed to modify or replace the PUREX process and meet new requirements such as the development of a one-cycle process without redox chemistry. Following the principle of interaction of O- or N-donor organic molecules with uranium or plutonium,[5,6] new types of complexing agents have been studied.

In France, the Group ActiNide EXtraction (GANEX) process has been developed for the industrial reprocessing of spent nuclear fuel and the homogeneous recycling of actinides.[7,8] In this process, the selective separation is operated by solvent extraction using a new group of the *N,N*-dialkyl amides (further monoamides) first appeared in the 1960s.[9–11] It has been demonstrated that monoamides have a strong affinity with both the uranyl and plutonium cations.[12–15] Their selectivity can be adjusted by varying either the length or the ramification of monoamide alkyl chain.[9,16,17] The use of *N,N*-di-(ethyl-2-hexyl)isobutyramide (DEHiBA) has been proposed for U(VI) recovery and U(VI)/Pu(IV) or U(VI)/Th(IV). The knowledge of the stoichiometries and coordination of the actinide cations in aqueous and organic media is of high importance not only to better understand the extraction mechanism but also to optimize the extraction efficiency and selectivity. In the case of uranyl extraction, it has been shown that the neutral complex $UO_2(NO_3)_2(L)_2$ forms in the organic phase.[18–20] It has a hexagonal bipyramidal geometry corresponding to the uranyl center to which two nitrates and two amide groups are linked as it has been confirmed by X-ray diffraction (XRD), Raman spectroscopy, and IR spectroscopy.[12,21] One should point out that the nitrates can be located either in *cis*- or *trans*-position. Although there are cases reported in the literature involving a *cis*-conformation around the uranyl moiety,[12,13,22] they are far less common than the *trans* conformation. As the two conformations exist in crystals, they might both be present in nitric acid solution and in organic phases.

The existence of different species could induce a change in the electronic structure of uranyl binitrate complexes. To reveal a difference in the coordination sphere of uranyl

in terms of the position of the nitrates and monoamides, the organic phase after extraction can be characterized by UV-vis or time-resolved laser-induced fluorescence spectroscopy (TRLFS). The latter method has some advantageous features, allowing us to measure luminescence spectra at a low total uranium concentration and discriminate side-emitting compounds by temporal resolution. Moreover, the positions of the luminescence bands, band spacings, bandwidths, and intensities are features that can be interpreted to determine the nature and the number of ligands in the first coordination layer of $UO_2{}^{2+}$, as well as the local symmetry of the complex. The determination of electronic structure information from the luminescence spectra is either still unresolved or it requires additional data. Previously, to study an electronic structure of the $UO_2Cl_4{}^{2-}$ complex, Görller-Warland et al.[23] used UV-vis and magnetic circular dichroism spectroscopies. Another way is to model theoretical spectra.[24–27]

As it has already been described previously,[24–29] to study the uranium-based complexes and interpret the experimental spectra, quantum chemical modeling is an insightful tool as it provides an accurate description of the electronic structure. Using the methodology described in our recent publications,[28,29] the luminescence spectra, as well as spectroscopic characteristics can be computed and used for the assignment of the experimental spectra. In our previous studies, the methodology has been proven to give an accurate description of the electronic structure of the uranyl complexes allowing us to elucidate and quantify the influence of the first and second coordination spheres on the luminescence features. The structural parameters, emission energies, and simulated luminescence spectra were found to be in good accordance with experimental data giving a significant level of confidence in the chosen theoretical methodology.

Here, we aim at studying the uranyl binitrate complexes and the influence of water and monoamide molecules in the first coordination sphere using quantum chemical simulations and the comparison to available and newly acquired experimental data. Theoretical models were created based on previous studies on the uranyl binitrate compounds[30,31] and will

be described in detail further. The structural parameters of uranyl binitrate models will be discussed at the relativistic PBE0 level of theory in their *cis* and *trans* configurations. For the sake of guiding future experimental studies on uranyl binitrate compounds, the stability and probability of the conformers have been computed. As the spin-orbit CAM-B3LYP method has been found to accurately place electron transition energies of actinide complexes,[32] it is used to determine the luminescence origin in experimental spectra since it is not obviously identified experimentally. Moreover, we expect that this study is not only useful in illustrating the broad applicability of quantum modeling but may also guide scientists in spectral data processing, i.e., identification of the bands and importance of their intensities.

Experimental details

Materials

DEHiBA was purchased from Pharmasynthese (purity $\geq 99\%$) and used as received. Hydrogenated tetrapropylene (TPH) used as a diluent was purchased from Novasep. The organic phases were prepared by dissolving weighed amounts of monoamide in TPH.

The U(VI) aqueous phase was prepared by dissolution of solid uranium(VI) nitrate hexahydrate ($UO_2(NO_3)_2 \cdot 6\,H_2O$) obtained from Prolabo (purity $\geq 99\,\%$) into a solution of $2\,\mathrm{mol\,L^{-1}}$ lithium nitrate (reagent grade) with deionized water produced by the Milli-Q Plus apparatus (Millipore). The pH was adjusted to 2 by adding a suitable volume of $1\,\mathrm{mol\,L^{-1}}$ nitric acid.

Liquid-liquid extraction

Suitable volumes of DEHiBA at a concentration of $1.5\,\mathrm{mol\,L^{-1}}$ in n-TPH were contacted with aqueous phases (V_{org}/V_{aq}). Extraction was performed at room temperature ($\approx 25\,^{\circ}\mathrm{C}$) with 30 min stirring. Then, the solution was centrifuged and separated for titration and

analytical procedures.

Uranyl concentrations were determined using the X-ray fluorescence technique (Thermo Scientific - ARL QUANT'X – EDRXRF Analyser). Samples were diluted in 1 mol L^{-1} DEHiBA in TPH. The calibration range of references solutions of uranyl nitrate in the same matrix is 100–2000 mg L^{-1}.

UV-vis Absorption Spectroscopy UV-vis measurements were performed on a Varian Cary 50 Scan spectrophotometer between 350 and 500 nm in quartz cells.

TRLFS Analysis

A narrow-band Nd-YAG/OPO/Fx1 laser (tripled Surelite 8010 and doubled sunlite EX from Continuum) was used as the excitation source. This solid-state laser is ideal for scanning any wavelength between 220 and 1800 nm (energies from 1 to 20 mJ). Fluorescence was observed at right angle to the excitation by an alignment of 8 Si/Si optical fibers illuminating the entrance slit of a flat-field spectrometer (300i from Princeton Instrument) equipped with a pulsed intensified CCD camera (IMAX, 1024×256 pixels, Princeton Instrument) synchronized on the laser shot.

To avoid the decomposition of the organic ligand by UV radiation, the OPO was tuned to 420 nm and controlled to generate 10 Hz repetition rate. Also, the laser pulse energy was decreased until the intensity of the fluorescence remained stable during the excitation, i.e. 0.6 mJ and the laser beam was defocused into the cell by a quartz lens. The optical system has been modified to defocus the laser beam to avoid its concentration at a single point of the sample. For this, a double compartment cell was used to attenuate the energy and the number of incident photons. The first cell contained the reference aqueous solution of uranyl nitrate 0.1 mol L^{-1} in 2 mol L^{-1} $LiNO_3$ pH=2 used for normalization of the spectra while the sample was in the second cell. The recording of spectra was performed by integration of the pulse light signal given by the intensifier with a time delay of 150 ns and during a determined

aperture time of 1 µs. Accumulation of 500 laser shots were averaged for each spectrum.

Computational Details

The choice of the used QM methods is justified in previous works.[28,29,33] The ground- and excited-state molecular geometries were optimized with Gaussian 16[34] software including scalar relativistic effects and using the PBE0 functional of the density.[35] For the $UO_2(NO_3)_2(H_2O)$ and *cis*-/*trans*–$UO_2(NO_3)_2(H_2O)_2$ complexes, the water solvent was accounted for using the continuum polarizable conductor model (CPCM)[36] ($\varepsilon_r = 78.36$). The experimentally studied *N,N*-di(2-ethylhexyl)-*iso*-butanamide (DEHiBA) molecule was transformed to the *N,N*-diethyl-*iso*-butanamide (DEiBA) molecule with a shorter alkyl chain, to keep the computational costs reasonable, as the original alkyl chain is located beyond the first coordination sphere of U(VI) and is expected not to affect the uranyl-core electronic structure.[28,31] The experimental luminescence spectrum of the $UO_2(NO_3)_2(DEHiBA)_2$ complex was recorded in hydrogenated tetrapropylene (TPH), which is an industrial solvent that is often described as branched dodecane; thus, one can assume that it has similar properties to that of *n*-dodecane, namely, a low polarity. Therefore, the structures of *cis*-/*trans*–$UO_2(NO_3)_2(DEiBA)_2$ complexes were optimized in the gas phase, as the solvent is expected not to induce sizable changes of the complex geometries because of its low permittivity value ($\varepsilon_r = 2.00$ taken for *n*-dodecane).[28] The geometries of the luminescent states (first triplet excited states) were optimized using the time-dependent density functional theory (TD-DFT)/PBE0 approach as implemented in Gaussian 16 code[34] with equilibrium solvation where it was necessary. The vibrational harmonic frequencies of the ground and luminescent states were computed analytically. All optimized geometries considered for the vibronic spectra calculations represent real minima as they have no imaginary frequencies. In these calculations, the def2-TZVP basis sets[37,38] were used for the H, C, N, and O elements. A small-core Relativistic Effective Core Potential (RECP) that accounts for scalar

relativistic effects of the 60 core electrons[39,40] was used for the uranium atom, while the valence electrons were described by the def-TZVP basis set.[41] To speed up the TD-DFT calculations within the Gaussian 16 package, the inner U(5s, 5p, 5d), O(1s), C(1s), N(1s) orbitals were frozen.

To compute accurate absolute energies of the electron transitions involved in the luminescence spectra of uranyl nitrate complexes, we have performed CAM-B3LYP[42] TD-DFT single-point calculations, at the spin-free excited-state structures, including spin-orbit coupling effects with the ZORA Hamiltonian,[43] and modeling the environment effect (water solvent for *cis*- and *trans*-$UO_2(NO_3)_2(H_2O)_n$ (n=1,2) and *n*-dodecane for $UO_2(NO_3)_2(DEiBA)_2$) with the conductor-like screening model COSMO.[44–46] These calculations were carried out with the Amsterdam Density Functional package (ADF 2018.01).[47] All atoms were described by TZ2P Slater-type basis sets[48] without freezing the atomic cores.

The theoretical luminescence spectra of uranium(VI) complexes have been computed with the `ezSpectrum 3.0`[49] software. The Franck-Condon factors (FCFs) were computed analytically including Duschinsky transformations of the normal modes between the ground and excited states. The number of vibrational quanta in the luminescent and ground state were selected to be one and five, respectively, to match the recorded experimental vibronic transitions. All of the vibronic progressions were computed at 300 K to include contributions from the thermally active vibrational modes. As the proposed quantum chemical methods cannot compute absolute intensities, the intensity of the electron transition peak was manually adjusted to match the experimental intensity distributions. The spectral shapes were estimated by convoluting the discrete stick spectra with Lorentzian broadening functions adjusting the width to match the experimental one.

Free energy calculations were performed using a composite method. While all of the entropic and vibrational contributions are obtained from the DFT calculations, the electronic energies are estimated either at the DFT/PBE0 or MP2 level of theory using the Turbomole 7.3[50] and the Gaussian 16.[34]

Choice of the Model Systems

In general, the coordination number of the uranyl unit varies from four to six depending on the nature of ligands and media.[51] In nitric acid solutions, the uranium(VI) speciation may be composed of several species like uranyl UO_2^{2+} and uranyl nitrate complexes ($UO_2(NO_3)_n^{(2-n)}$, n = 1, 2) that has been detected by TRLFS.[52] In organic media, the uranyl nitrate complex is soluble as a neutral compound $UO_2(NO_3)_2(L)_2$.[31] As one of the main goals of this study is to elucidate the influence of organic ligands present in the first coordination sphere, the chemical model systems should have the same coordination number and molecular charge. In the present work, the majority of the model systems are 6-fold coordinated and are neutral. The structures are shown in Figure 1. In the crystal phase, the uranyl nitrate complex hydration shell contains six water molecules, but there are at most two water molecules in the first coordination sphere, $[UO_2(NO_3)_2(H_2O)_2] \cdot 4\,H_2O$.[53] As the $UO_2(NO_3)_2$ molecule has a coordination of four, with the two bidentate nitrate groups coordinated to uranyl, we have added one or two water molecules in the uranyl equatorial plane (1) to check the influence of the number of water molecules on the $UO_2(NO_3)_2(H_2O)_n$ ($n = 1, 2$) complexes spectra and emission energies, and (2) to quantify the relative stability of *cis*-/*trans*–$UO_2(NO_3)_2(H_2O)_2$ conformers (see Table S1 in the Supporting Information, SI). Hereafter, the two water molecules were substituted by two *N,N*-diethyl-*iso*-butanamide (DEiBA) , which is truncated *N,N*-di(2-ethylhexyl)-*iso*-butanamide (DEHiBA).

Results

Theoretical Ground and Excited-State Structures

cis-/*trans*–$UO_2(NO_3)_2(H_2O)_n$ (n=1, 2)

All of the distances for the $UO_2(NO_3)_2(H_2O)$ and *cis*-/*trans*–$UO_2(NO_3)_2(H_2O)_2$ complexes are reported in Table 1 along with experimental data available in the literature. The ground-

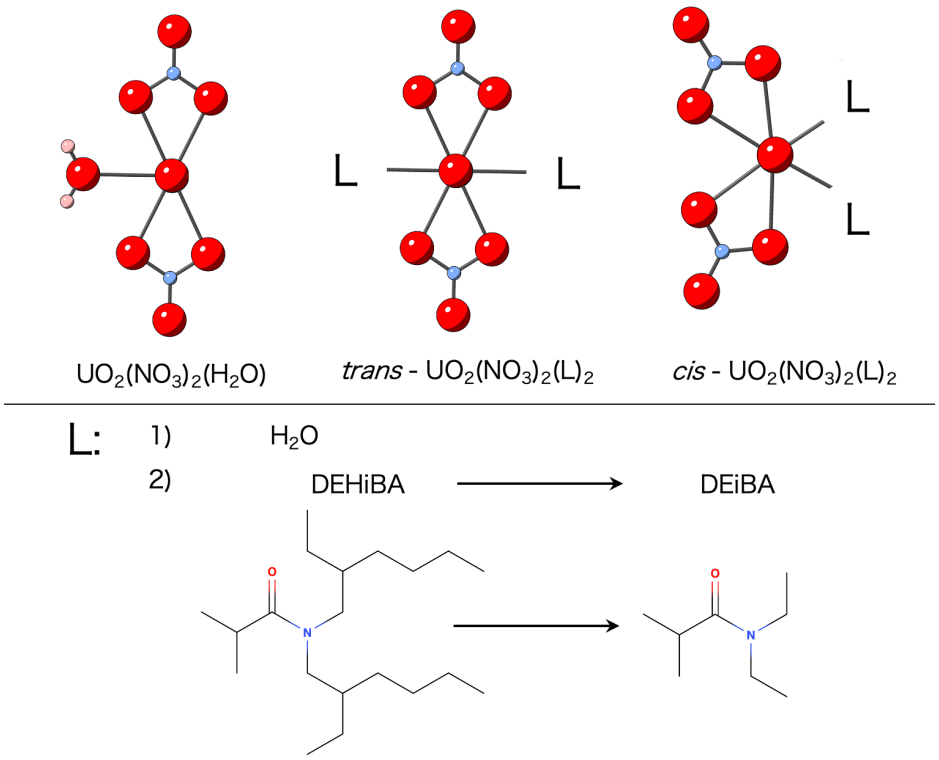

Figure 1: Structures of $UO_2(NO_3)_2(H_2O)$ and $UO_2(NO_3)_2(L)_2$ (L=H_2O, DEiBA) model systems in their *trans*- and *cis*-configurations. The view is made along the z-axis defined by the uranyl moiety.

state structures of these complexes are found to be almost identical with a maximum deviation of 0.003 Å for $U-O_{ax}$, $U-O_{NO_3}$ and $U-N_{NO_3}$ bond lengths. The $U-O_{H_2O}$ bond is 0.024 Å longer in the *trans*$-UO_2(NO_3)_2(H_2O)_2$ complex than in the $UO_2(NO_3)_2(H_2O)$ complex, as there are more electrostatic repulsions in the former than in the latter. Taylor et al.[54] obtained nonequivalent $U-O_{ax}$ bond distances (1.770(7) and 1.749(7) Å), while in our calculations, these distances are strictly equal (1.749 Å). We suspect the experimental bond length difference to be related to the fit uncertainty because most of the uranyl complexes have almost equivalent $U-O_{ax}$ bond lengths.[55,56] The *trans*$-UO_2(NO_3)_2(H_2O)_2$ complex structure has been studied previously by theoretical DFT/SVWN[57] and Car-Parrinello (CP/BLYP) calculations.[58] The results obtained by these two methods overestimate the

bond lengths found in the crystal structures by neutron diffraction measurements,[54] whereas our DFT/PBE0 ground-state structures are in better agreement with the experimental structural data. These compiled results indicate that the choices of both the functional and the basis sets have a significant impact on the accuracy of the geometries of computed U(VI)-based complexes. Comparing the structures of *cis*- and *trans*–$UO_2(NO_3)_2(H_2O)_2$ conformers, we did not observe any significant change in the structures except for the $U-O_{H_2O}$ bond, which was found to be 0.014 Å longer in the *cis* conformer than in the *trans*. This is probably related to the greater energetic stability of the *trans* complex as shown in Table S1 in the SI.

The geometrical parameters of the lowest triplet excited states are also reported in Table 1. As a result of the electron excitation, we observe an elongation of the $U-O_{ax}$ bond length by 0.038 Å for the uranyl binitrate complex with one water molecule and 0.037 Å for both *cis*- and *trans*–$UO_2(NO_3)_2(H_2O)_2$ conformers. For the equatorial ligands, the structural changes are found to be very minor, suggesting that there are no significant contributions of the water ligands to the orbitals participating to the excitation.

Insofar as vibrational frequencies contribute to the luminescence spectra to some extent, it is of high importance to characterize them. There are three main vibrational modes that may appear in the vibronic progressions: uranyl bending ν_b, symmetrical stretching ν_s and asymmetrical stretching ν_a modes. The values of these frequencies are reported in Table 2 together with the experimental IR and Raman data obtained for solid[59] and liquid[30] uranyl binitrates. The analysis of the theoretical harmonic frequencies of $UO_2(NO_3)_2(H_2O)$ and *cis*-/*trans*–$UO_2(NO_3)_2(H_2O)_2$ complexes shows nearly the same results being overestimated by at most 62 cm^{-1} for the uranyl symmetrical stretching mode compared to experimental data. Also, our calculations showed that the ν_b mode is coupled with the motions of ligands, an information that cannot be deduced from the IR spectra of $UO_2(NO_3)_2$ in solution.[30] It is thus inappropriate to describe this vibrational frequency as a pure uranyl bending mode. Experimentally, it was measured at 254 cm^{-1}, matching the range of our computed values

Table 1: Ground and Excited-State Geometries (in Å) of $UO_2(NO_3)_2(H_2O)$ and *cis-*/*trans*$-UO_2(NO_3)_2(L)_2$ (L=H_2O, DEiBA) Compared to Selected Results from the Literature[a]

	U$-O_{ax}$	U$-O_{NO3}$	U$-N_{NO3}$	U$-O_L$	Method	Ref.
			Ground State			
$UO_2(NO_3)_2(H_2O)$	1.746	2.473	2.917	2.474	PBE0/CPCM	this study
trans$-UO_2(NO_3)_2(H_2O)_2$	1.749	2.470	2.914	2.498	PBE0/CPCM	this study
cis$-UO_2(NO_3)_2(H_2O)_2$	1.749	2.469	2.914	2.512	PBE0/CPCM	this study
trans$-UO_2(NO_3)_2(DEiBA)_2$	1.756	2.496	2.945	2.390	PBE0/GP	this study
cis$-UO_2(NO_3)_2(DEiBA)_2$	1.755	2.480	2.929	2.441	PBE0/GP	this study
trans$-UO_2(NO_3)_2(H_2O)_2$	1.749(7)	2.504(5)		2.397(3)	neutrons	[54]
	1.770(7)	2.547(7)			diffraction	
	1.820	2.530		2.550	CP/ZORA(aq)	[58]
	1.800	2.490		2.590	CP/BLYP/ECP60	[58]
$UO_2(NO_3)_2(DEHiBA)_2$	1.77(1)	2.53(1)	2.97(3)	2.38(2)	EXAFS	[31]
cis$-UO_2(NO_3)_2(dam)_2$	1.760(3)	2.533(3)	-	2.362(3)	X-ray	[12]
trans$-UO_2(NO_3)_2(eam)_2$	1.747(3)	2.526(4)	-	2.363(3)	X-Ray	[12]
			Excited state			
$UO_2(NO_3)_2(H_2O)$	1.784	2.479	2.921	2.479	PBE0/CPCM	this study
trans$-UO_2(NO_3)_2(H_2O)_2$	1.786	2.476	2.918	2.500	PBE0/CPCM	this study
cis$-UO_2(NO_3)_2(H_2O)_2$	1.786	2.473	2.918	2.515	PBE0/CPCM	this study
trans$-UO_2(NO_3)_2(DEiBA)_2$	1.792	2.515	2.963	2.375	PBE0/GP	this study
cis$-UO_2(NO_3)_2(DEiBA)_2$	1.791	2.495	2.943	2.428	PBE0/GP	this study

[a] dam - N',N-diethylacetamide; eam - N-ethylacetamide.

217–276 cm^{-1}.

Table 2: Ground and Excited State Vibrational Frequencies (in cm^{-1}) of the $UO_2(NO_3)_2(H_2O)$ and *cis*-/*trans*–$UO_2(NO_3)_2(L)_2$ (L=H_2O, DEiBA) Compared to Selected Results from the Literature$^A NALYSIS$

	ν_b	ν_s	ν_a	Method	Ref.
			Ground state		
$UO_2(NO_3)_2(H_2O)$	217-276	934	989	PBE0/CPCM	this study
trans–$UO_2(NO_3)_2(H_2O)_2$	230-264	925	978	PBE0/CPCM	this study
cis–$UO_2(NO_3)_2(H_2O)_2$	217-265	928	980	PBE0/CPCM	this study
trans–$UO_2(NO_3)_2(DEiBA)_2$	280	911	987	PBE0/GP	this study
cis–$UO_2(NO_3)_2(DEiBA)_2$	278	913	989	PBE0/GP	this study
$UO_2(NO_3)_2$	254	872	961	IR/Raman	[30]
$UO_2(NO_3)_2(H_2O)_2$		875	945	IR/Raman	[59]
$UO_2(NO_3)_2(DEiBA)_2$			935	IR	[14]
cis–$UO_2(NO_3)_2(dam)_2$			923	IR	[12]
trans–$UO_2(NO_3)_2(eam)_2$			932	IR	[12]
			Excited state		
$UO_2(NO_3)_2(H_2O)$	210-267	833	856	PBE0/CPCM	this study
trans–$UO_2(NO_3)_2(H_2O)_2$	220-257	833	857	PBE0/CPCM	this study
cis–$UO_2(NO_3)_2(H_2O)_2$	223-261	834	857	PBE0/CPCM	this study
trans–$UO_2(NO_3)_2(DEiBA)_2$	275	822	850	PBE0/GP	this study
cis–$UO_2(NO_3)_2(DEiBA)_2$	270	823	850	PBE0/GP	this study

[a] dam - N',N-diethylacetamide; eam - N-ethylacetamide.

As a result of the U–O_{ax} bond elongation from the ground to the luminescent state, the ν_s and ν_a vibrational frequencies are lowered by 101 cm^{-1} and 133 cm^{-1}, respectively, in the *trans*–$UO_2(NO_3)_2(H_2O)$ complex. A similar behavior is observed for *cis*-/*trans*–$UO_2(NO_3)_2(H_2O)_2$ complexes. One can, however, note that the coupled ν_b frequency range is not significantly affected by the excitation process.

cis-/*trans*–$UO_2(NO_3)_2(DEiBA)_2$

To probe the electronic structure of U(VI) surrounded by inorganic and organic ligands, two molecules of the DEiBA monoamide were placed in the first coordination sphere instead of the water molecules forming $UO_2(NO_3)_2(DEiBA)_2$ *cis*- and *trans*-conformers (Fig. 2). The

optimized bond distances are shown in Table 1. The substitution of water molecules by the DEiBA monoamide ligands induces a lengthening of the U$-$O$_{ax}$, U$-$O$_{NO_3}$ and U$-$N$_{NO_3}$ bonds while the distance between uranium and the oxygen atom of the monoamide is shorter than that with the oxygens of the water molecules, by 0.108 Å and 0.071 Å for the *trans* and *cis* configurations, respectively. This is simply a result of the larger electron donation to uranium by the DEiBA monoamide compared to water.[31]

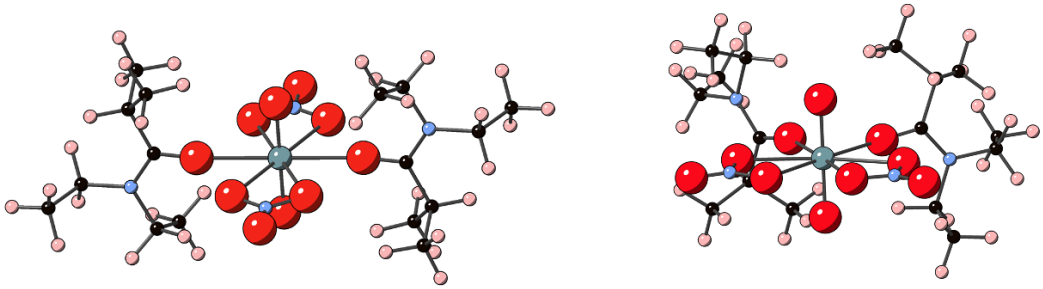

Figure 2: Optimized at R-ECP DFT/PBE0 ground-state geometries of *cis*- and *trans*-$UO_2(NO_3)_2(DEiBA)_2$ conformers.

The ground-state geometries of the *cis*- and *trans*-$UO_2(NO_3)_2(DEiBA)_2$ complexes have very similar distances in the equatorial plane, and the free energy difference of two conformers is small. Nevertheless, the *trans* conformer is found to be more stable compared to *cis*, by about 23 kJ mol^{-1} and 15 kJ mol^{-1} at the DFT/PBE0 and MP2 levels of theory, respectively (see Table S1 in the SI). The computed geometry of the *trans*-$UO_2(NO_3)_2(DEiBA)_2$ complex agrees well with the experimental EXAFS results obtained by Acher et al.[31] In the same way, the computed bond lengths within $UO_2(NO_3)_2(DEiBA)_2$ conformers also agree with the single-crystal X-ray structures of similar amide compounds like *cis*$-UO_2(NO_3)_2(dam)_2$ (dam - N',N-diethylacetamide) and *trans*$-UO_2(NO_3)_2(eam)_2$ (eam - N-ethylacetamide).[12]

The changes in the geometries when switching from the ground to the luminescent state in *cis*- / *trans*-$UO_2(NO_3)_2(DEiBA)_2$ complexes are of the same order as that reported for the *cis*- / *trans*-$UO_2(NO_3)_2(H_2O)_2$ complexes.

The theoretical vibrational frequencies of *cis*- and *trans*-$UO_2(NO_3)_2(DEiBA)_2$ complexes are listed in Table 2. As in aqueous complexes, there is almost no difference for the ν_b, ν_s and ν_a frequencies between the *cis* and *trans* conformers. Moreover, the ν_b frequency corresponds to a pure uranyl bending motion, uncoupled from the equatorial ligands, ν_s is smaller and ν_a remains almost unchanged. The changes are most probably related to the weakening of the $U-O_{ax}$ bond paired with the decrease in uranyl stretching force constant. The calculated ν_a frequency can be compared with experimental data measured by IR spectroscopy for various crystals and liquid samples of *cis*- / *trans*-$UO_2(NO_3)_2(L)_2$ complexes.[12,31] As observed for the $UO_2(NO_3)_2(H_2O)_2$ complexes, our theoretical vibrational frequencies for the $UO_2(NO_3)_2(DEiBA)_2$ complexes are overall larger than the experimental values by $65\,cm^{-1}$. Thus, this systematic difference might be related to choice of the computational methodology (DFT functional, basis sets, and/or solvation model).[33,60,61]

The changes between the ground- and the luminescent states vibrational frequencies in the *cis*-/*trans*-$UO_2(NO_3)_2(DEiBA)_2$ complexes are equal, on average, to $90\,cm^{-1}$ and $138\,cm^{-1}$ for the symmetrical and asymmetrical uranyl stretching modes, respectively, while the ν_b frequency is similar to that in the ground state.

Emission energies

For the uranyl-based complexes, the nature of the luminescent emission was previously discussed in several experimental[62–64] and theoretical[65–67] studies. It was deduced from the examples of uranyl tetrachloride $UO_2Cl_4^{2-}$ [28] and uranyl triscarbonate $UO_2(CO_3)_3^{4-}$ [29] complexes that the luminescent state has a triplet character and that the emission occurs as a result of an electron transition from one of the four nonbonding 5f orbitals of uranium(VI) to an orbital that has a uranyl σ character possibly mixed with orbitals of the equatorial ligands. In the present $UO_2(NO_3)_3(L)_2$ complexes, the plots of the molecular orbitals involved in the luminescent process shown in Figure 3 reveal that the emission corresponds to a metal-to-ligand charge transfer deexcitation from nonbonding uranium(VI) orbitals to

orbitals delocalized over the uranyl unit, the nitrate ligands, and the monoamide linking groups.

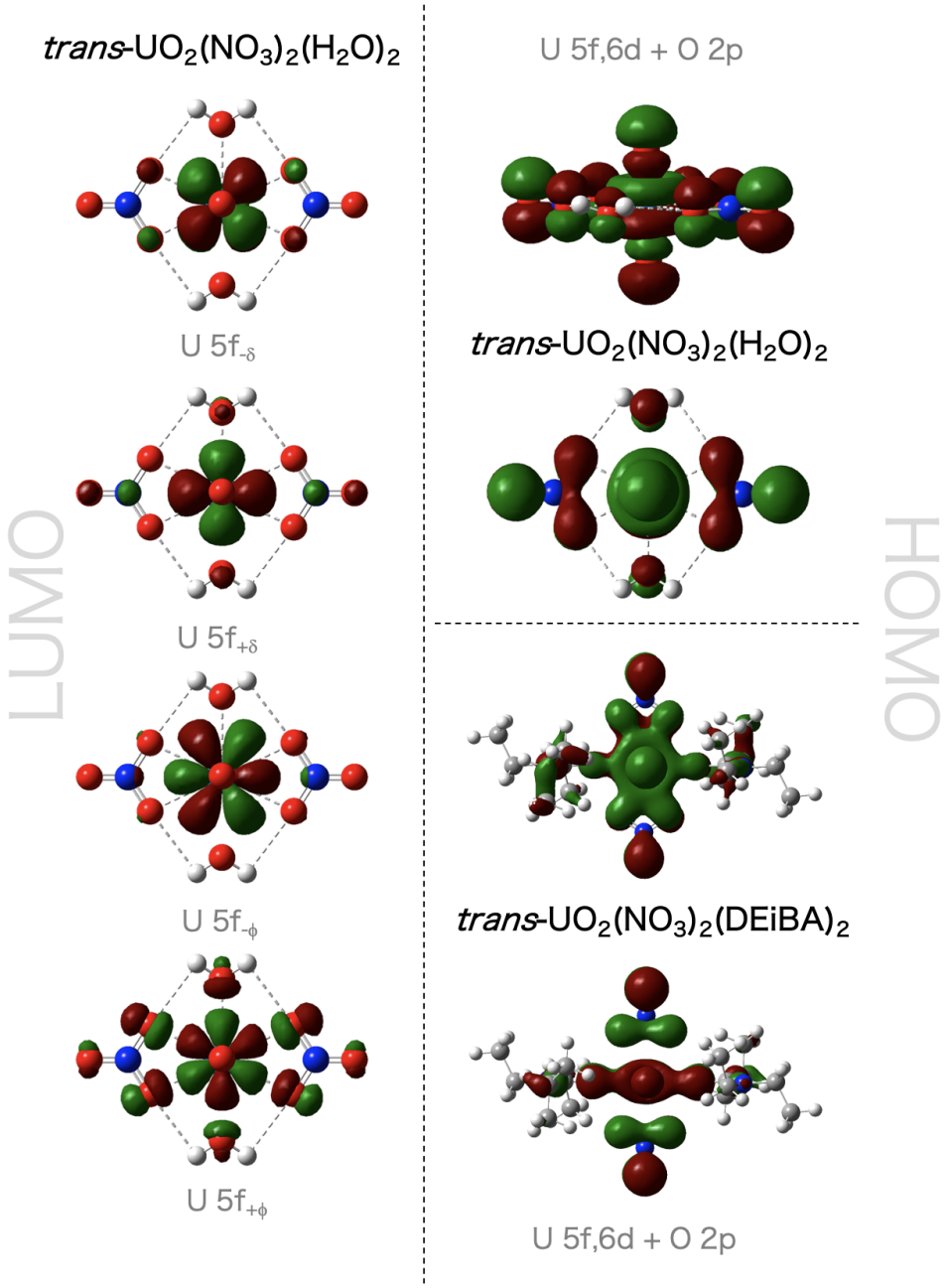

Figure 3: Highest occupied (right) and lowest unoccupied (left) molecular orbitals of *trans*-$UO_2(NO_3)_2(L)_2$ (L = H_2O, DEiBA) involved in the triplet-singlet electron transitions, responsible for uranyl luminescence. The molecular orbitals were obtained at the RECP DFT/PBE0 level of theory computed for the singlet ground state.

Since the luminescence spectra of uranyl-based complexes have similar shapes (with some

exceptions like $UO_2Cl_4^{2-}$), the nature of the equatorial ligands can be deduced from the position of the spectral envelope in the energy scale.[23,24,68] In the luminescence spectra, the origin is usually defined by the position of the electron transition. For instance, luminescence blue shifts of the uranyl triscarbonate complexes are observed as compared to most other uranyl species, while hydrated uranyl exhibits a redshift.[68–70] It has been proposed by Wang et al.[68] that the origin of luminescence in uranyl minerals depends on the basicity of the equatorial ligand. The ionic interactions between uranyl ion and ligands with higher pK_a lead to a larger decrease of the ν_s frequency and a larger redshift of the luminescence spectra.

Here, we have used the SOC CAM-B3LYP calculations to predict the luminescence origin by averaging the first four vertical emission energies computed out of the first low-lying excited-state geometry and corrected by the zero-point energies of the ground and luminescent states of the $UO_2(NO_3)_2(H_2O)$ and *cis-* / *trans*-$UO_2(NO_3)_2(L)_2$ (L=H_2O, DEiBA).[71] The computed energies E are listed in Table 3. The comparison of theoretical data with experimental results is not relevant at this stage, because to our knowledge, the position of the electron transition was never discussed before for the uranyl binitrate complexes.

The theoretical electronic transition energies of the $UO_2(NO_3)_2(H_2O)$ and *cis-*/*trans*-$UO_2(NO_3)_2(H_2O)_2$ complexes in water come out close, within 413 cm^{-1} (10 nm). These differences are within the expected accuracy of our quantum chemical methodology. Notwithstanding, we restrict ourselves to making a comparison with the results obtained for compounds with different basicities of equatorial ligands. Within the uranyl binitrate water complexes with one or two coordinated water molecules, since the equatorial plane does not differ by the nature of the ligands (it means that basicity remains unchanged), we can take an average energy value of $UO_2(NO_3)_2(H_2O)$, *cis-*/*trans*-$UO_2(NO_3)_2(H_2O)_2$ and compare it to the $Na_3UO_2(CO_3)_3^-$ complex value.[29] It is known from the study by Parr and Pearson et al.[72] that nitrates and water molecules are less basic than the carbonate anions. From our calculations, the luminescence origin of $Na_3UO_2(CO_3)_3^-$ is placed at 21 412 cm^{-1}

Table 3: Electron Transition Energies E of Uranyl Binitrate Complexes (in cm^{-1} and nm) Compared to $Na_3UO_2(CO_3)_3^-$ and $[A336]_2[UO_2Cl_4]$ Results[a]

	E [cm^{-1}]	E [nm]
Water COSMO		
$UO_2(NO_3)_2(H_2O)$	20204	495
trans–$UO_2(NO_3)_2(H_2O)_2$	20456	489
cis–$UO_2(NO_3)_2(H_2O)_2$	20616	485
$Na_3UO_2(CO_3)_3^-$	20978	477
n-dodecane COSMO		
trans–$UO_2(NO_3)_2(DEiBA)_2$	20116	497
cis–$UO_2(NO_3)_2(DEiBA)_2$	20171	496
$[A336]_2[UO_2Cl_4]$	20001	500

[a] The computed values are obtained at the all-electron SOC CAM-B3LYP level of theory and corrected with the spin-free zero-point energy correction of the ground and luminescent states.

(467 nm), while the averaged energy value for the uranyl binitrate is 20 425 cm^{-1} (490 nm), showing 987 cm^{-1} (23 nm) redshift which is consistent with Wang's assumption.[68]

For the *cis*- and *trans*-$UO_2(NO_3)_2(DEiBA)_2$ (for which the basicity is not known yet) in *n*-dodecane, we have computed the electron transition energies at 20 116 cm^{-1} (497 nm) and 20 171 cm^{-1} (496 nm), respectively. They are somewhat red-shifted with respect to that of the water complexes of uranyl binitrate. Compared to the energy value of the $[A336]_2[UO_2Cl_4]$ complex, 20 001 cm^{-1} (500 nm), the uranyl binitrates with monoamides electron transition energy exhibit a blueshift.

One can notice that the *cis*- and *trans*-conformers of uranyl binitrate complexes may hardly be discriminated solely by the electron emission energy.

Vibronic Progressions

In the luminescent emission of U(VI) complexes, the principal vibronic progression is a result of an electron transition coupled to the symmetrical stretching mode of the uranyl unit. Secondary progressions may also appear to some extent because of the coupling to other

symmetrical motions of the uranyl binitrate monoamide complexes. The quantum chemical simulations of the vibronic spectra allow to quantify the contributions of the vibronic modes. To guide the discussion and the comparison to experimental data, the computed stick spectra of all binitrate uranyl complexes are convoluted and shown in Figure 4.

The structural and vibrational parameters directly reflect in the shape of the luminescence spectra. The most evident and easily detectable fingerprint is the ground-state symmetrical stretching mode of the uranyl moiety, as it is equal to the spacing between the main peaks of the vibronically resolved envelope. Some other vibrational frequencies (symmetrical mostly) appear in the vibronic progression to a smaller extent and might hardly be detected in the broad spectral envelope. The contribution of vibrational frequencies and their natures and intensities are listed in Table 4 for the $UO_2(NO_3)_2(H_2O)$ and *cis*-/ *trans*-$UO_2(NO_3)_2(L)_2$ (L = H_2O, DEiBA) complexes. One can note that the excited-state uranyl symmetrical stretching mode can be detected in these luminescence spectra as discussed further.

The ground-state symmetrical stretching uranyl frequency has been discussed previously. From the comparison of the spectra displayed in Figure 4 and the symmetric stretching frequencies listed in Table 4, we can infer that the vibronic band spacings are very similar; thus, the spectra of aqueous and organic uranyl binitrate complexes are difficult to separate solely by the main vibronic band spacings. The detailed analysis of the vibronic bands reveals that some other modes build up a secondary vibronic progression. In the case of the $UO_2(NO_3)_2(H_2O)$ complex, the uranyl rocking appears at $156\,cm^{-1}$ after the first band. In the *cis*- and *trans*-$UO_2(NO_3)_2(H_2O)_2$ spectra, we observe contributions from the U$-$$H_2O$ stretching mode coupled to uranyl bending motions at $249\,cm^{-1}$ and $315\,cm^{-1}$ for the *cis*- and *trans*-conformers, respectively. A symmetrical U$-$$NO_3$ stretching mode coupled with the weak uranyl bending motion contributes to the spectra of the *cis*- and *trans*-$UO_2(NO_3)_2(DEiBA)_2$ complexes at $234\,cm^{-1}$ and $212\,cm^{-1}$, respectively.

The theoretical luminescence intensities distribution are mainly linked to the U$-$$O_{ax}$ bond elongations between the ground and luminescent states,[27] but this relationship is not

Table 4: Assignments of the $UO_2(NO_3)_2(H_2O)$ and *cis-*/ *trans*-$UO_2(NO_3)_2(L)_2$ (L = H_2O, DEiBA) Theoretical Luminescence Spectra Computed in the Gas Phase and in the CPCM Water Solvent for Complexes with Organic and Inorganic Ligands Respectively[a,b,c,d]

E [cm^{-1}]	ΔE [cm^{-1}]	I [au]	E [cm^{-1}]	ΔE [cm^{-1}]	I [au]	Identification
$UO_2(NO_3)_2(H_2O)$						
19831		0.347				0'(0)→0(0)
19675	156	0.061				0'(0)→0(1ν_1)
18897	934	0.138				0'(0)→0(1ν_s)
18741	156	0.018				0'(0)→0(1ν_1,1ν_s)
17963	934	0.037				0'(0)→0(2ν_s)
17807	156	0.004				0'(0)→0(1ν_1,2ν_s)
17028	935	0.008				0'(0)→0(3ν_s)
16094	934	0.001				0'(0)→0(4ν_s)
trans−$UO_2(NO_3)_2(H_2O)_2$			*cis*−$UO_2(NO_3)_2(H_2O)_2$			
20104		0.531	20344		0.424	0'(0)→0(0)
19789	315	0.005	20095	249	0.014	0'(0)→0(1ν_2)
19179	925	0.291	19417	927	0.236	0'(0)→0(1ν_s)
18864	315	0.003	19167	249	0.008	0'(0)→0(1ν_2,1ν_s)
18255	924	0.096	18489	927	0.080	0'(0)→0(2ν_s)
17645	315	0.000	18240	249	0.003	0'(0)→0(1ν_2,2ν_s)
17330	925	0.024	17562	927	0.021	0'(0)→0(3ν_s)
16405	925	0.005	16634	927	0.005	0'(0)→0(4ν_s)
trans−$UO_2(NO_3)_2(DEiBA)_2$			*cis*−$UO_2(NO_3)_2(DEiBA)_2$			
19674		0.097	19850		0.313	0'(0)→0(0)
19462	212	0.007	19616	234	0.011	0'(0)→0(1ν_3)
18763	911	0.047	18937	913	0.158	0'(0)→0(1ν_s)
18551	212	0.003	18703	234	0.007	0'(0)→0(1ν_3,1ν_s)
17852	911	0.014	18024	913	0.049	0'(0)→0(2ν_s)
17640	212	0.000	17790	234	0.002	0'(0)→0(1ν_3,2ν_s)
16942	911	0.003	17111	913	0.012	0'(0)→0(3ν_s)

[a] The energy of the spectrum was adjusted to the theoretical E value and corrected by ν_s of the excited state.

[b] ν_1 is uranyl rocking, ν_2 is U−H_2O stretching + weak ν_b,

[c] ν_3 is U−NO_3 stretching + weak ν_b

[d] 0' and 0 are the luminescent and ground electronic level notations, respectively, while the vibronic-level notation is defined within parentheses.

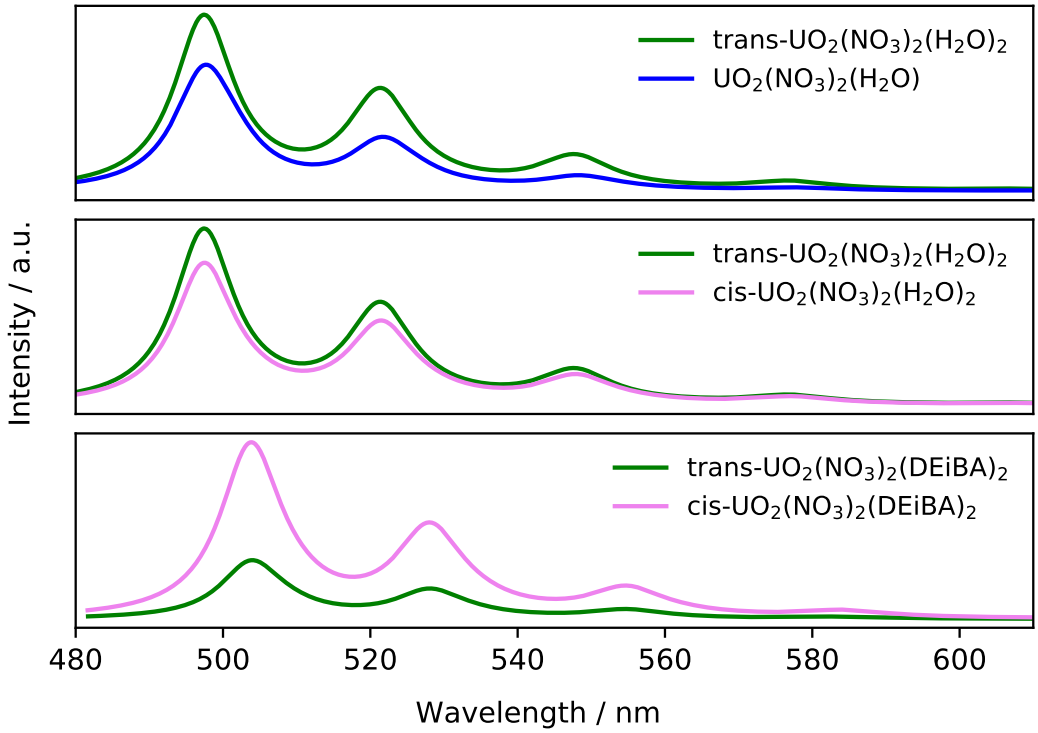

Figure 4: Theoretical vibronic progressions (in nm, see SI for cm^{-1}) of the $UO_2(NO_3)_2(H_2O)$ and *cis*-/ *trans*-$UO_2(NO_3)_2(L)_2$ (L = H_2O, DEiBA) complexes. The position of the spectral envelope is adjusted to the computed emission energies the *trans* -complexes. The spectral shapes were estimated by convoluting the stick spectra with Lorentzian functions with a an full width at half maximum (FWHM) of 400 cm^{-1} and presented in wavelength scale.

defined yet. We have performed a comparison of the vibronic progressions to elucidate the influence of the nature of the ligands and of their orientations on theoretical intensities. In Figure 4 (top) we observe that the absolute intensity of the *trans*-$UO_2(NO_3)_2(H_2O)_2$ complex is higher than that of $UO_2(NO_3)_2(H_2O)$ by 0.184 au for the first band. Figure 4 (middle) reveals that the *trans*-conformer of uranyl binitrate with two water molecules exhibits higher intensities than the *cis* conformer by 0.107 au. In Figure 4 (bottom), the spectra of *cis*- and *trans*-$UO_2(NO_3)_2(DEiBA)_2$ have been compared and, unlike in the uranyl binitrate water complexes, the spectrum of the *cis* conformer is more intense by 0.216 au than the *trans*-one. From the analysis of the geometries and the shifts from the ground to the luminescent state, we did not find any significant difference, especially in the $U-O_{ax}$ bond. It means that

intensity change is not related here to the geometrical changes discussed earlier, but rather to some other factors. As the vibronic intensities arise from the Franck-Condon overlaps between the ground- and excited-state normal modes, if they are not parallel, Duschinsky rotations need to be accounted for, and may contribute to the intensity changes.

Discussions

As for most of the U(VI) compounds, the luminescence spectra of the uranyl nitrate complexes show well-resolved vibronic progressions that overlap with the pure electron transition from the luminescent state to the ground state. We have collected TRLFS experimental data for $UO_2(NO_3)_2$ in nitric acid (plain line),[52] $UO_2(NO_3)_2(DEHiBA)_2$ in TPH solvent (dotted line) and $UO_2(NO_3)_2(TBP)_2$ in supercritical CO_2 (dashed line).[73] The normalized experimental luminescence emission spectra are shown in Figure 5.

The different complexes of uranium(VI) in nitric acid aqueous solution produce several luminescence components with similar monoexponential luminescent decay. The individual components are thus difficult to separate by using the time resolution of the detection. The picture becomes less complicated in the presence of organic extracting agent (like TBP or monoamides) when the uranyl binitrate complexes can be present as a single species and only potentially conformers.

To the best of our knowledge, there is no information in the literature about the nature of observed transitions in the uranyl binitrate complexes. The general observation that the vibronic progression overlaps with the electron transition can be interpreted in different ways. In the example of the emission spectrum of the $UO_2(NO_3)_2(DEHiBA)_2$ complex (Figure 5 and Figure 6) we observe two peaks in the high-energy region at 480–495 nm with different intensities. It is known that the intensity of luminescence depends on the quantum yield – the ratio of the rate of deexcitation by photon emission to the rate of deexcitation by both radiative and nonradiative processes.[27] For this particular case, it is difficult not only

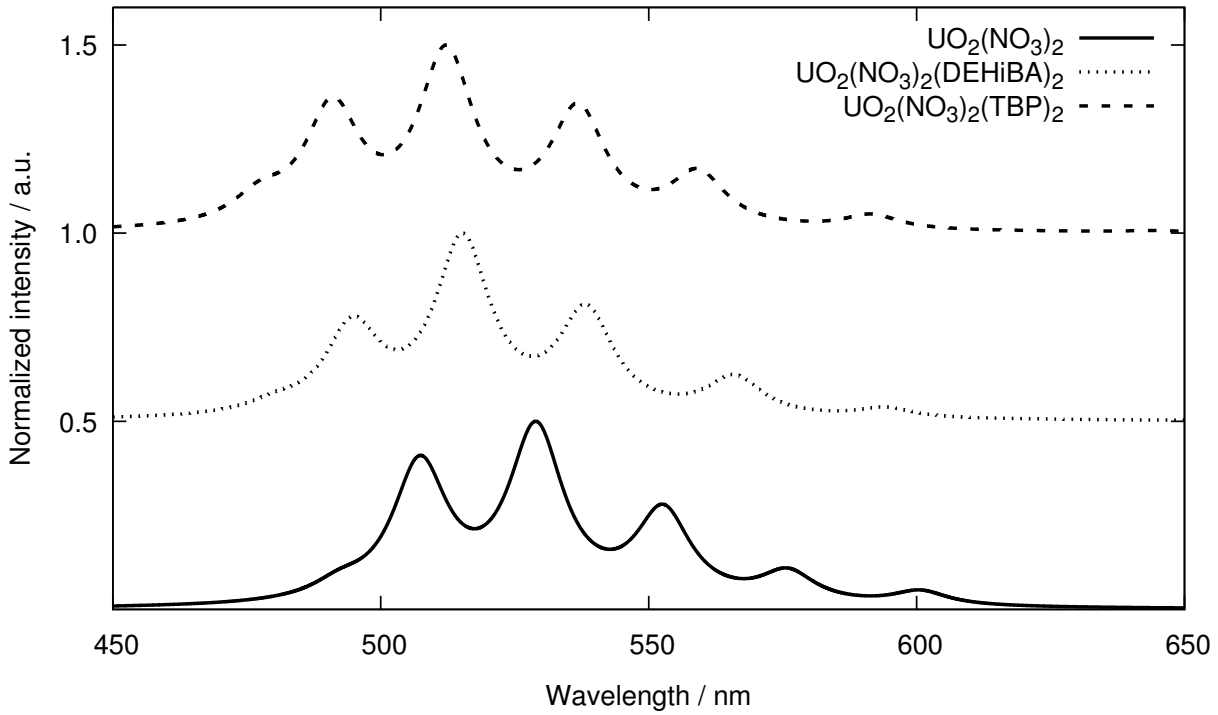

Figure 5: Experimental luminescence emission spectra of $UO_2(NO_3)_2$ in nitric acid[52] (plain lines), $UO_2(NO_3)_2(DEHiBA)_2$ in TPH solvent, ε=2.0 (dotted line) and $UO_2(NO_3)_2(TBP)_2$ in a supercritical CO_2, ε=1.6[73] (dashed line). The spectra were rebuilt from the data of the quoted references.

to determine the origin of the relaxation but also to predict the temporal evolution of the electron intensity; thus, both transitions could correspond to the electron one. Usually, when the absorption and emission spectra are built on the same energy scale, they overlap at the electron transition region as shown in Figure 6. Here, we notice the overlay of the same two peaks around 480 and 495 nm. Using the analogy adverted by Görller-Warland et al.[23] on the example of uranyl chloride complexes, the first small peak at 480 nm could be assigned to a "hot band" $1'(0) \rightarrow 0(0)$, while the second at 495 nm should correspond to the main $0'(0) \rightarrow 0(0)$ electron transition between the excited and the ground states of the complex (dashed line in Figure 6).

Another way to attribute the position of the main transition in $UO_2(NO_3)_2(L)_2$ is to use the band spacing value and results obtained by *ab initio* calculations. In the luminescence spectrum, the vibronic progression starts at the $0'(0) \rightarrow 0(0)$ transition with a spacing equal

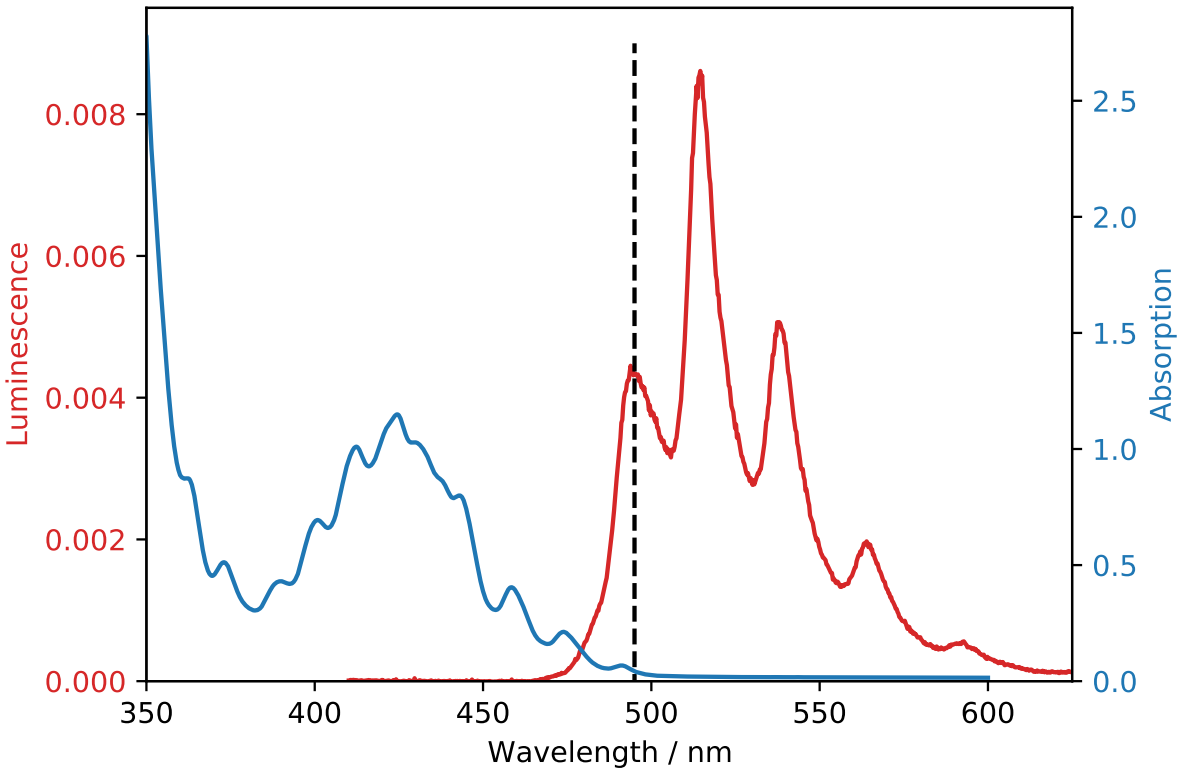

Figure 6: Superposition of the emission (TRLFS) and absorption (UV-vis) spectra of $UO_2(NO_3)_2(DEHiBA)_2$ in TPH solvent of the same sample.

to the ground-state uranyl stretching frequency ν_s^{gs}. The hot band appears at an energy shifted by the excited state uranyl stretching frequency ν_s^{es} above the electron transition. A multipeak Lorentzian fitting was applied to the experimental spectra to determine the band spacing values. The results of this fitting and the ν_s^{gs}, ν_s^{es} frequencies computed by (TD)-DFT/PBE0 methods are shown in Table 5.

It has been observed that for $UO_2(NO_3)_2(L)_2$ complexes, the experimental ground- and excited-state symmetrical stretching frequencies of the uranyl reproduced the theoretical trend that the ν_s^{gs} frequency is larger than the ν_s^{es}. Moreover, the ν_s^{gs} extracted from the luminescence spectra agreed within $11\,cm^{-1}$ with Raman data for $UO_2(NO_3)_2(H_2O)_2$ in liquid.[30] The shifts between the ground and excited state stretching frequencies $\Delta\nu_s$ are 65 and $49\,cm^{-1}$ for the $UO_2(NO_3)_2$ and $UO_2(NO_3)_2(DEHiBA)_2$, respectively, while the theoretical shifts equal to $90\,cm^{-1}$ in average. As it has been explained in previous works,[28,29]

our theoretical methodology tends to overestimate the vibrational frequency values; thus, we can consider that the agreement between theoretical and experimental data is satisfactory. Moreover, it is difficult to estimate the degree of anharmonicity effects in experimental spectra, which might obviously decrease the band spacings in the low-energy region.

Table 5: Experimental and Theoretical Spectral Characteristics of Uranyl Binitrate Complexes[a]

L	$0'(0) \rightarrow 0'(n)$ maxima (nm) n=0	n=1	n=2	n=3	n=4	ν_s^{gs} [cm^{-1}]	ν_s^{es} [cm^{-1}]
Experimental							
H_2O[52]	507	529	554			864	799
DEHiBA	495	516	540	566	593	844	795
Theoretical							
trans-H_2O [a]	507	529	557	587	621	925	833
cis-H_2O [a]	507	529	557	587	621	928	834
trans-DEiBA [b]	495	516	542	570	601	911	822
cis-DEiBA [b]	495	516	542	570	601	913	823

[a] The peak maxima are reported in nm. Experimental ν_s^{gs} and ν_s^{es} values were obtained by a Lorentzian fitting procedure. The ν_s^{gs} corresponds to the averaged band spacing values between the vibronic transitions; ν_s^{es} corresponds to spacing between the $0'(0) \rightarrow 0(0)$ and $1'(0) \rightarrow 0(0)$ transitions. ν_s^{gs} and ν_s^{es} are given in cm^{-1}

[b] $0'(0) \rightarrow 0'(0)$ was taken from experimental $UO_2(NO_3)_2(L)_2$ (L = H_2O, DEHiBA) emission spectra to match position of theoretical peaks with experimental ones.

Based on the discussions above, we have tried to attribute the electronic and vibronic transitions of experimental spectra being guided by the theoretical results. The direct comparison of our theoretical spectra with the experimental ones can be visualized in Figure 7, the spectral characteristics and attribution of bands are listed in Table 5. To simplify the discussion, we have shifted the theoretical spectra to match the experimental energy range and normalized the intensities of both sets to the maximum value. First of all, the difference between the ν_s^{gs} and ν_s^{es} experimental values leads us to propose that the $0'(0) \rightarrow 0(0)$ band pops up at 507 and 495 nm for $UO_2(NO_3)_2(H_2O)_2$ and $UO_2(NO_3)_2(DEHiBA)_2$, respectively. Another remarkable result is that the theoretical vibronic progression intensity distribution

exactly match the experimental ones when placing them next to the proposed band. The bands at 495 and 480 nm in $UO_2(NO_3)_2(H_2O)_2$ and $UO_2(NO_3)_2(DEHiBA)_2$, respectively, are the "hot bands" $1'(0) \rightarrow 0(0)$ whose vibronic progression might contribute to the intensity of the electron transition on the spectrum.

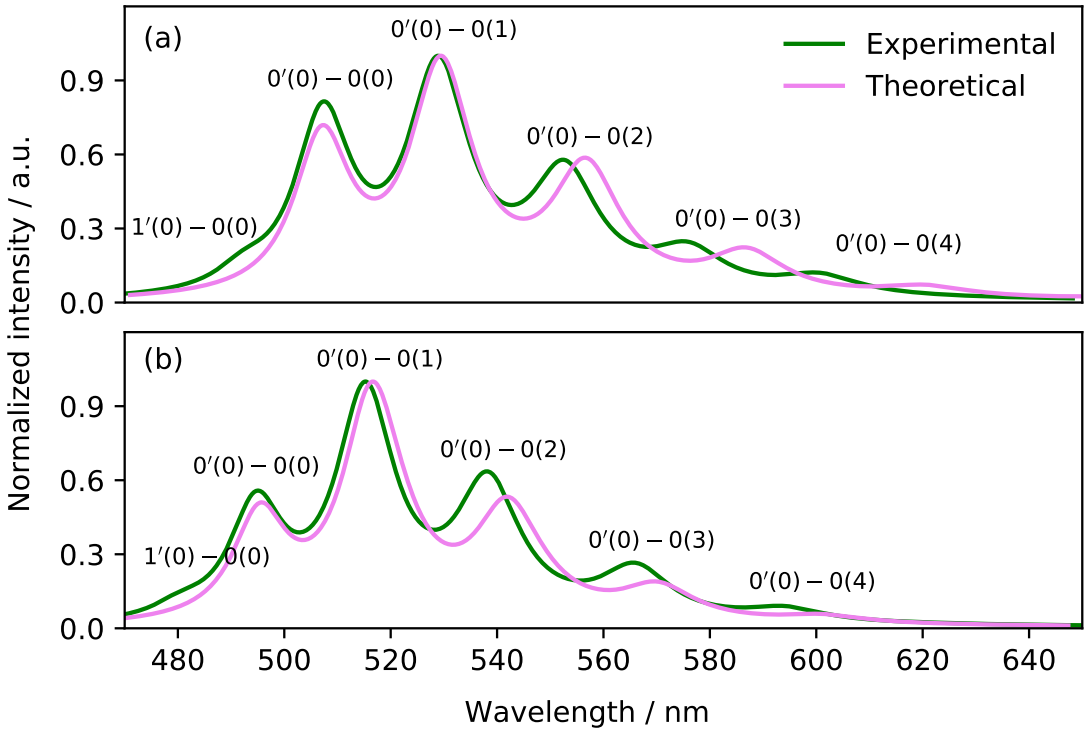

Figure 7: Comparison of experimental luminescence emission spectra with theoretical spectra of (a) $UO_2(NO_3)_2(H_2O)_2$ and (b) $UO_2(NO_3)_2(DEiBA)_2$. The notation explanation is provided in SI.

One last point that was not yet discussed in detail is the detection probability of the *cis*- and *trans*-conformers of uranyl binitrate complexes to distinguish them from the experimental luminescence data. When we discussed the differences in the structures (Table 1) and harmonic frequencies (Table 2) of both conformers, the same as predicted luminescence spectra (Table 5), it was difficult to distinguish the more probable configuration of the $UO_2(NO_3)_2(H_2O)_2$ and $UO_2(NO_3)_2(DEiBA)_2$. Furthermore, the relative free energies between the two conformers (see Table S1 of SI) are found to be very small to give an

exact picture. Nevertheless, the *cis-trans* energetic difference data predicted the *cis*- and *trans*-isomers to be probable by about 30 % and 70%, respectively, for the uranyl binitrate complexes with water, and *trans*–$UO_2(NO_3)_2(DEiBA)_2$ complex to be 100% probable. This kind of analysis represents a static picture only, while under the experimental conditions, the systems are dynamics, with possible rapid exchanges between conformers.

Conclusions

The speciation of uranyl in solution can be investigated by TRLFS to determine the species that may dominate or coexist. This requires an accurate decomposition scheme and experimental data of high quality. In the context of spent fuel reprocessing, monoamide molecules are developed to selectively extract uranium(VI) from the aqueous to the organic phase. The present work by TRLFS and *ab initio* based methodology shows that no significant change is to be expected in the electronic structure of the uranium binitrate moiety. PBE0 (TD)-DFT approach accurately captured the ground- and excited-state structures with minor discrepancies, which can probably be attributed to the choice of the functional of the density, the basis set, and the solvation model. The proposed theoretical methodology allowed to calculate the main vibronic progression of the complexes with the corresponding assignment of the electron transitions and vibrational modes involved, showing that PBE0 (TD)-DFT is an effective tool for prediction and assignment of luminescent spectra of U(VI)-based complexes.

In this work, we have used a stepwise growth of the chemical models to assess the sensitivity to the number of water molecules in the coordination sphere of uranyl and by substituting the water molecules with monoamide DEiBA. Using the chemical models in a form of $UO_2(NO_3)_2(H_2O)$ and *cis-*/*trans*-$UO_2(NO_3)_2(L)_2$(L = H_2O, DEiBA) it has been confirmed that the structural and spectroscopic parameters exhibit similar and hardly distinguishable features. Structural isomers for a given stoichiometry are indeed energetically very close and have almost identical luminescence emission spectra. Calculations of luminescence bands

intensities were found to be in excellent agreement with experimental spectra, giving confidence in the validity of our methodology. This approach could be emphasized for a deeper interpretation of the data from time-resolved laser-induced fluorescent spectroscopy, which is often efficiently used to track changes in the first coordination sphere of uranyl unit.

Acknowledgement

The authors acknowledge support by the French government through the Program "Investissement d'avenir" (LABEX CaPPA / ANR-11-LABX-0005-01 and I-SITE ULNE / ANR-16-IDEX-0004 ULNE), as well as by the Ministry of Higher Education and Research, Hauts de France council and European Regional Development Fund (ERDF) through the Contrat de Projets État-Région (CPER CLIMIBIO). Furthermore, this work was granted access to the HPC resources of [CINES/IDRIS/TGCC] under the allocation 2020–2021 [A0090801859] made by GENCI. The authors also acknowledge the CEA for the Ph.D. grant attributed to H.O.

Supporting Information Available

The Supporting Information file supplemental-uo2no3.pdf is available free of charge. It contains:

- Relative free energies of the *trans*- or *cis* isomers computed in the gas phase and in the CPCM water solvent at the PBE0 and MP2 levels of theory (Table S1);
- Spectra in cm^{-1} corresponding to Figure 4 (in nm) (Figure S1);
- Notations for Figure 7 (Figure S2) (PDF)

References

(1) Taylor, R. *Reprocessing and Recycling of Spent Nuclear Fuel*; Elsevier, 2015.

(2) Moyer, B. A. *Ion Exchange and Solvent Extraction: A Series of Advances, Volume 19*; CRC Press, 2009.

(3) Boullis, B.; Baron, P. *Modelling of Uranium/plutonium Splitting in Purex Process*; 1987; p 9.

(4) Saab, M.; Réal, F.; Šulka, M.; Cantrel, L.; Virot, F.; Vallet, V. Facing the Challenge of Predicting the Standard Formation Enthalpies of N-Butyl-Phosphate Species with Ab Initio Methods. *J. Chem. Phys.* **2017**, *146*, 244312, DOI: 10.1063/1.4986953.

(5) Madic, C.; Lecomte, M.; Baron, P.; Boullis, B. Separation of Long-Lived Radionuclides from High Active Nuclear Waste. *C. R. Physique* **2002**, *3*, 797–811, DOI: 10.1016/S1631-0705(02)01370-1.

(6) Dinh, B.; Baron, P.; Duhamet, J. In *Le Traitement-Recyclage Du Combustible Nucléaire Usé*; Lecomte, M., Bonin, B., Eds.; CEA Saclay et Groupe Moniteur (Éditions du Moniteur): Paris, 2008; pp 55–70.

(7) Adnet, J.-M.; Miguirditchian, M.; Hill, C.; Heres, X.; Lecomte, M.; Masson, M.; Brossard, P.; Baron, P. Development of New Hydrometallurgical Processes for Actinide Recovery: GANEX Concept. Proceedings of GLOBAL. Tsukuba, Ibaraki (Japan), 2005.

(8) Miguirditchian, M.; Sorel, C.; Camès, B.; Bisel, I.; Baron, P.; Espinoux, D.; Calor, J.; Viallesoubranne, C.; Lorrain, B.; Masson, M. Ha Demonstration in the Atalante Facility of the Ganex 1st Cycle for the Selective Extraction of Uranium from HLW. Proceedings of GLOBAL. 2009; pp 1032–1035.

(9) Siddall III, T. Effects of Structure of N, N-Disubstituted Amides on Their Extraction

of Actinide and Zirconium Nitrates and of Nitric Acid1. *J. Phys. Chem.* **1960**, *64*, 1863–1866, DOI: 0.1021/j100841a014.

(10) Fritz, J. S.; Orf, G. M. Extraction of Metal Ions with N, N-Disubstituted Amides. *Anal. Chem.* **1975**, *47*, 2043–2045, DOI: 10.1021/ac60362a008.

(11) Gasparini, G. M.; Grossi, G. Review Article Long Chain Disubstituted Aliphatic Amides As Extracting Agents in Industrial Applications of Solvent Extraction. *Solvent Extr. Ion Exch.* **1986**, *4*, 1233–1271, DOI: 10.1080/07366298608917921.

(12) Loubert, G.; Volkringer, C.; Henry, N.; Arab-Chapelet, B.; Delahaye, T.; Loiseau, T. Structural Studies of a Series of Uranyl Alkylacetamides and Piracetam Complexes Obtained in Nitric Acid Aqueous Solution. *Polyhedron* **2017**, *138*, 7–12, DOI: 10.1016/j.poly.2017.09.006.

(13) Deb, S.; Gamare, J.; Kannan, S.; Drew, M. Uranyl (VI) and Lanthanum (III) Thio-Diglycolamides Complexes: Synthesis and Structural Studies Involving Nitrate Complexation. *Polyhedron* **2009**, *28*, 2673–2678, DOI: 10.1016/j.poly.2009.06.001.

(14) Moeyaert, P.; Dumas, T.; Guillaumont, D.; Kvashnina, K.; Sorel, C.; Miguirditchian, M.; Moisy, P.; Dufrêche, J.-F. Modeling and Speciation Study of Uranium (VI) and Technetium (VII) Coextraction with DEHiBA. *Inorg. Chem.* **2016**, *55*, 6511–6519, DOI: 10.1021/acs.inorgchem.6b00595.

(15) Pathak, P. N.; Kumbhare, L. B.; Manchanda, V. K. Structural Effects in N, N-Dialkyl Amides on Their Extraction Behavior Toward Uranium and Thorium. *Solvent Extr. Ion Exch.* **2001**, *19*, 105–126, DOI: 10.1081/SEI-100001377.

(16) Nair, G. M.; Prabhu, D. R.; Mahajan, G. R. Extraction of Uranium (VI) and Plutonium (IV) with Dihexylbutyramide and Dihexylisobutyramide from Nitric Acid Medium. *J. Radioanal. Nucl. Chem.* **1994**, *182*, 393–399, DOI: 10.1007/bf02037516.

(17) Prabhu, D. R.; Mahajan, G. R.; Nair, G. M. Di (2-Ethyl Hexyl) Butyramide and Di (2-Ethyl Hexyl) Isobutyramide As Extractants for Uranium (VI) and Plutonium (IV). *J. Radioanal. Nucl. Chem.* **1997**, *224*, 113–117, DOI: 10.1007/bf02034622.

(18) Condamines, N.; Musikas, C. The Extraction by NN-Dialkylamides. II. Extraction of Actinide Cations. *Solvent Extr. Ion Exch.* **1992**, *10*, 69–100, DOI: 10.1080/07366299208918093.

(19) Vasudevan, T.; Murali, M. S.; Nagar, M. S.; Mathur, J. N. Extraction of U (VI) from Nitrate and Thiocyanate Media with Monoamides. *Solvent Extr. Ion Exch.* **2002**, *20*, 665–686, DOI: 10.1081/SEI-120016072.

(20) Rodrigues, F.; Ferru, G.; Berthon, L.; Boubals, N.; Guilbaud, P.; Sorel, C.; Diat, O.; Bauduin, P.; Simonin, J. P.; Morel, J. P.; Morel-Desrosiers, N.; Charbonnel, M. C. New Insights into the Extraction of Uranium(VI) by an N,N-Dialkylamide. *Mol. Phys.* **2014**, *112*, 1362–1374, DOI: 10.1080/00268976.2014.902139.

(21) Wahu, S.; Berthet, J.-C.; Thuéry, P.; Guillaumont, D.; Ephritikhine, M.; Guillot, R.; Cote, G.; Bresson, C. Structural Versatility of Uranyl (VI) Nitrate Complexes That Involve the Diamide Ligand Et_2N (C= O)$(CH_2)_n$(C=O) NEt_2 (0 - N - 6). *Eur. J. Inorg. Chem.* **2012**, *2012*, 3747–3763, DOI: 10.1002/ejic.201200243.

(22) Kannan, S.; Deb, S. B.; Drew, M. G. Synthesis, Structural and Emission Studies of a Bis (carbamoyl Methyl) Sulfone Complex of Uranyl Nitrate. *Inorg. Chem. Commun.* **2011**, *14*, 225–227, DOI: 10.1016/j.inoche.2010.10.028.

(23) Görller-Walrand, C.; De Houwer, S.; Fluyt, L.; Binnemans, K. Spectroscopic Properties of Uranyl Chloride Complexes in Non-Aqueous Solvents. *Phys. Chem. Chem. Phys.* **2004**, *6*, 3292–3298, DOI: 10.1039/B317002K.

(24) Drobot, B.; Steudtner, R.; Raff, J.; Geipel, G.; Brendler, V.; Tsushima, S. Combining Luminescence Spectroscopy, Parallel Factor Analysis and Quantum Chemistry to

Reveal Metal Speciation–a Case Study of Uranyl (VI) Hydrolysis. *Chem. Sci.* **2015**, *6*, 964–972, DOI: 10.1039/C4SC02022G.

(25) Su, J.; Wang, Z.; Pan, D.; Li, J. Excited States and Luminescent Properties of UO_2F_2 and Its Solvated Complexes in Aqueous Solution. *Inorg. Chem.* **2014**, *53*, 7340–7350, DOI: 10.1021/ic5006852.

(26) Su, J.; Wang, Y.-L.; Wei, F.; Schwarz, W.; Li, J. Theoretical Study of the Luminescent States and Electronic Spectra of UO_2Cl_2 in an Argon Matrix. *J. Chem. Theory Comput.* **2011**, *7*, 3293–3303, DOI: 10.1021/ct200419x.

(27) Su, J.; Zhang, K.; Schwarz, W. E.; Li, J. Uranyl-Glycine-Water Complexes in Solution: Comprehensive Computational Modeling of Coordination Geometries, Stabilization Energies, and Luminescence Properties. *Inorg. Chem.* **2011**, *50*, 2082–2093, DOI: 10.1021/ic200204p.

(28) Oher, H.; Réal, F.; Vercouter, T.; Vallet, V. Investigation of the Luminescence of $[UO_2X_4]^{2-}$ (X = Cl, Br) Complexes in the Organic Phase Using Time-Resolved Laser-Induced Fluorescence Spectroscopy and Quantum Chemical Simulations. *Inorg. Chem.* **2020**, *59*, 5896–5906, DOI: 10.1021/acs.inorgchem.9b03614.

(29) Oher, H.; Vercouter, T.; Réal, F.; Shang, C.; Reiller, P. E.; Vallet, V. Influence of Alkaline Earth Metal Ions on Structures and Luminescent Properties of $Na_mMe_nUO_2(CO_3)_3^{(4-M-2n)-}$ (Me = Mg, Ca; M, N = 0-2): Time-Resolved Fluorescence Spectroscopy and Ab Initio Studies. *Inorg. Chem.* **2020**, *59*, 15036–15049, DOI: 10.1021/acs.inorgchem.0c01986.

(30) Gál, M.; Goggin, P. L.; Mink, J. Mid-, Far-Infrared and Raman Spectra of Uranyl Complexes in Aqueous Solutions. *J. Mol. Struct.* **1984**, *114*, 459–462, DOI: 10.1016/0022-2860(84)87186-0.

(31) Acher, E.; Hacene Cherkaski, Y.; Dumas, T.; Tamain, C.; Guillaumont, D.; Boubals, N.; Javierre, G.; Hennig, C.; Solari, P. L.; Charbonnel, M.-C. Structures of Plutonium (IV) and Uranium (VI) with N, N-Dialkyl Amides from Crystallography, X-Ray Absorption Spectra, and Theoretical Calculations. *Inorg. Chem.* **2016**, *55*, 5558–5569, DOI: 10.1021/acs.inorgchem.6b00592.

(32) Tecmer, P.; Gomes, A. S. P.; Ekström, U.; Visscher, L. Electronic Spectroscopy of UO_2^{2+}, NUO^+ and NUN: An Evaluation of Time-Dependent Density Functional Theory for Actinides. *Phys. Chem. Chem. Phys.* **2011**, *13*, 6249–6259, DOI: 10.1039/C0CP02534H.

(33) Tecmer, P.; Bast, R.; Ruud, K.; Visscher, L. Charge-Transfer Excitations in Uranyl Tetrachloride ($[UO_2Cl_4]^{2-}$): How Reliable Are Electronic Spectra from Relativistic Time-Dependent Density Functional Theory? *J. Phys. Chem. A* **2012**, *116*, 7397–7404, DOI: 10.1021/jp3011266.

(34) Frisch, M. J.; Trucks, G. W.; Schlegel, H. B.; Scuseria, G. E.; Robb, M. A.; Cheeseman, J. R.; Scalmani, G.; Barone, V.; Petersson, G. A.; Nakatsuji, H.; Li, X.; Caricato, M.; Marenich, A. V.; Bloino, J.; Janesko, B. G.; Gomperts, R.; Mennucci, B.; Hratchian, H. P.; Ortiz, J. V.; Izmaylov, A. F.; Sonnenberg, J. L.; Williams-Young, D.; Ding, F.; Lipparini, F.; Egidi, F.; Goings, J.; Peng, B.; Petrone, A.; Henderson, T.; Ranasinghe, D.; Zakrzewski, V. G.; Gao, J.; Rega, N.; Zheng, G.; Liang, W.; Hada, M.; Ehara, M.; Toyota, K.; Fukuda, R.; Hasegawa, J.; Ishida, M.; Nakajima, T.; Honda, Y.; Kitao, O.; Nakai, H.; Vreven, T.; Throssell, K.; Montgomery, J. A., Jr.; Peralta, J. E.; Ogliaro, F.; Bearpark, M. J.; Heyd, J. J.; Brothers, E. N.; Kudin, K. N.; Staroverov, V. N.; Keith, T. A.; Kobayashi, R.; Normand, J.; Raghavachari, K.; Rendell, A. P.; Burant, J. C.; Iyengar, S. S.; Tomasi, J.; Cossi, M.; Millam, J. M.; Klene, M.; Adamo, C.; Cammi, R.; Ochterski, J. W.; Martin, R. L.; Morokuma, K.; Farkas, O.;

Foresman, J. B.; Fox, D. J. Gaussian 16 Revision B.01. 2016; Gaussian Inc. Wallingford CT.

(35) Ernzerhof, M.; Scuseria, G. E. Assessment of the Perdew–Burke–Ernzerhof Exchange-Correlation Functional. *J. Chem. Phys.* **1999**, *110*, 5029–5036, DOI: 10.1063/1.478401.

(36) Tomasi, J.; Mennucci, B.; Cammi, R. Quantum Mechanical Continuum Solvation Models. *Chem. Rev.* **2005**, *105*, 2999–3094, DOI: 10.1021/cr9904009.

(37) Weigend, F.; Häser, M.; Patzelt, H.; Ahlrichs, R. RI-MP2: Optimized Auxiliary Basis Sets and Demonstration of Efficiency. *Chem. Phys. Lett.* **1998**, *294*, 143–152, DOI: 10.1016/S0009-2614(98)00862-8.

(38) Weigend, F.; Ahlrichs, R. Balanced Basis Sets of Split Valence, Triple Zeta Valence and Quadruple Zeta Valence Quality for H to Rn: Design and Assessment of Accuracy. *Phys. Chem. Chem. Phys.* **2005**, *7*, 3297–3305, DOI: 10.1039/B508541A.

(39) Küchle, W.; Dolg, M.; Stoll, H.; Preuss, H. Energy-Adjusted Pseudopotentials for the Actinides. Parameter Sets and Test Calculations for Thorium and Thorium Monoxide. *J. Chem. Phys.* **1994**, *100*, 7535–7542, DOI: 10.1063/1.466847.

(40) Cao, X.; Dolg, M.; Stoll, H. Valence Basis Sets for Relativistic Energy-Consistent Small-Core Actinide Pseudopotentials. *J. Chem. Phys.* **2003**, *118*, 487–496, DOI: 10.1063/1.1521431.

(41) Eichkorn, K.; Weigend, F.; Treutler, O.; Ahlrichs, R. Auxiliary Basis Sets for Main Row Atoms and Transition Metals and Their Use to Approximate Coulomb Potentials. *Theor. Chim. Acta* **1997**, *97*, 119–124, DOI: 10.1007/s002140050244.

(42) Yanai, T.; Tew, D. P.; Handy, N. C. A New Hybrid Exchange–Correlation Functional

Using the Coulomb-Attenuating Method (CAM-B3LYP). *Chem. Phys. Lett.* **2004**, *393*, 51–57, DOI: 10.1016/j.cplett.2004.06.011.

(43) Deetlefs, M.; Hussey, C. L.; Mohammed, T. J.; Seddon, K. R.; van den Berg, J.-A.; Zora, J. A. Uranium Halide Complexes in Ionic Liquids: An Electrochemical and Structural Study. *Dalton Trans.* **2006**, 2334–2341, DOI: 10.1039/B512212K.

(44) Klamt, A.; Schüürmann, G. COSMO: A New Approach to Dielectric Screening in Solvents with Explicit Expressions for the Screening Energy and Its Gradient. *J. Chem. Soc., Perkin Trans. 2* **1993**, *5*, 799–805, DOI: 10.1039/P29930000799.

(45) Klamt, A. Conductor-like Screening Model for Real Solvents: A New Approach to the Quantitative Calculation of Solvation Phenomena. *J. Phys. Chem.* **1995**, *99*, 2224–2235, DOI: 10.1021/j100007a062.

(46) Klamt, A.; Jonas, V. Treatment of the Outlying Charge in Continuum Solvation Models. *J. Chem. Phys.* **1996**, *105*, 9972–9981, DOI: 10.1063/1.472829.

(47) Baerends, E. J.; Ziegler, T.; Atkins, A. J.; Autschbach, J.; Bashford, D.; Baseggio, O.; Bérces, A.; Bickelhaupt, F. M.; Bo, C.; Boerritger, P. M.; Cavallo, L.; Daul, C.; Chong, D. P.; Chulhai, D. V.; Deng, L.; Dickson, R. M.; Dieterich, J. M.; Ellis, D. E.; van Faassen, M.; Ghysels, A.; Giammona, A.; van Gisbergen, S. J. A.; Goez, A.; Götz, A. W.; Gusarov, S.; Harris, F. E.; van den Hoek, P.; Hu, Z.; Jacob, C. R.; Jacobsen, H.; Jensen, L.; Joubert, L.; Kaminski, J. W.; van Kessel, G.; König, C.; Kootstra, F.; Kovalenko, A.; Krykunov, M.; van Lenthe, E.; McCormack, D. A.; Michalak, A.; Mitoraj, M.; Morton, S. M.; Neugebauer, J.; Nicu, V. P.; Noodleman, L.; Osinga, V. P.; Patchkovskii, S.; Pavanello, M.; Peeples, C. A.; Philipsen, P. H. T.; Post, D.; Pye, C. C.; Ramanantoanina, H.; Ramos, P.; Ravenek, W.; Rodríguez, J. I.; Ros, P.; Rüger, R.; Schipper, P. R. T.; Schlüns, D.; van Schoot, H.; Schreckenbach, G.; Seldenthuis, J. S.; Seth, M.; Snijders, J. G.; Solà, M.; M., S.; Swart, M.; Swerhone, D.;

te Velde, G.; Tognetti, V.; Vernooijs, P.; Versluis, L.; Visscher, L.; Visser, O.; Wang, F.; Wesolowski, T. A.; van Wezenbeek, E. M.; Wiesenekker, G.; Wolff, S. K.; Woo, T. K.; Yakovlev, A. L. ADF2018, SCM, Theoretical Chemistry, Vrije Universiteit, Amsterdam, the Netherlands, Https://www.scm.com.

(48) van Lenthe, E.; Baerends, E. J. Optimized Slater-Type Basis Sets for the Elements 1–118. *J. Comput. Chem.* **2003**, *24*, 1142–1156, DOI: 10.1002/jcc.10255.

(49) Mozhayskiy, V.; Krylov, A. EzSpectrum, Http://iopenshell.usc.edu/downloads. http://iopenshell.usc.edu/downloads.

(50) TURBOMOLE V7.3 2018, a Development of University of Karlsruhe and Forschungszentrum Karlsruhe GmbH, TURBOMOLE GmbH, Since 2007; Available from Http://www.turbomole.com. 1989-2007.

(51) Grenthe, I.; Drożdżyński, J.; Fujino, T.; Buck, E. C.; Albrecht-Schmitt, T. E.; Wolf, S. F. *The Chemistry of the Actinide and Transactinide Elements*; Chapter 5, pp 253–698, DOI: 10.1007/978-94-007-0211-0_5.

(52) Moulin, C.; Decambox, P.; Mauchien, P.; Pouyat, D.; Couston, L. Direct Uranium (VI) and Nitrate Determinations in Nuclear Reprocessing by Time-Resolved Laser-Induced Fluorescence. *Anal. Chem.* **1996**, *68*, 3204–3209, DOI: 10.1021/ac9602579.

(53) Field, B.; Hardy, C. Inorganic Nitrates and Nitrato-Compounds. *Q. Rev. Chem. Soc.* **1964**, *18*, 361–388, DOI: 10.1039/QR9641800361.

(54) Taylor, J. C.; Mueller, M. H. A Neutron Diffraction Study of Uranyl Nitrate Hexahydrate. *Acta Cryst.* **1965**, *19*, 536–543, DOI: 10.1107/S0365110X65003857.

(55) Watkin, D. J.; Denning, R. G.; Prout, K. Structure of Dicaesium Tetrachlorodioxouranium (VI). *Acta Crystallogr. C* **1991**, *47*, 2517–2519, DOI: 10.1107/S0108270191006777.

(56) Wilson, R. E.; Skanthakumar, S.; Cahill, C.; Soderholm, L. Structural Studies Coupling X-Ray Diffraction and High-Energy X-Ray Scattering in the UO_2^{2+}–HBr_{aq} System. *Inorg. Chem.* **2011**, *50*, 10748–10754, DOI: 10.1021/ic201265s.

(57) de Jong, W. A.; Apra, E.; Windus, T. L.; Nichols, J. A.; Harrison, R. J.; Gutowski, K. E.; Dixon, D. A. Complexation of the Carbonate, Nitrate, and Acetate Anions with the Uranyl Dication: Density Functional Studies with Relativistic Effective Core Potentials. *J. Phys. Chem. A* **2005**, *109*, 11568–11577, DOI: 10.1021/jp0541462.

(58) Bühl, M.; Kabrede, H.; Diss, R.; Wipff, G. Effect of Hydration on Coordination Properties of Uranyl (VI) Complexes. a First-Principles Molecular Dynamics Study. *J. Am. Chem. Soc.* **2006**, *128*, 6357–6368, DOI: 10.1021/ja057301z.

(59) McGlynn, S.; Smith, J.; Neely, W. Electronic Structure, Spectra, and Magnetic Properties of Oxycations. III. Ligation Effects on the Infrared Spectrum of the Uranyl Ion. *J. Chem. Phys.* **1961**, *35*, 105–116, DOI: 10.1063/1.1731876.

(60) Faulques, E.; Kalashnyk, N.; Massuyeau, F.; Perry, D. Spectroscopic Markers for Uranium (VI) Phosphates: A Vibronic Study. *RSC Adv.* **2015**, *5*, 71219–71227, DOI: 10.1039/C5RA13558C.

(61) Kovács, A.; Konings, R. J. Computed Vibrational Frequencies of Actinide Oxides $AnO^{0/+/2+}$ and $AnO_2^{0/+/2+}$ (An= Th, Pa, U, Np, Pu, Am, Cm). *J. Phys. Chem. A* **2011**, *115*, 6646–6656, DOI: 10.1021/jp202538k.

(62) Denning, R.; Snellgrove, T.; Woodwark, D. The Electronic Structure of the Uranyl Ion: Part I. the Electronic Spectrum of $Cs_2UO_2Cl_4$. *Mol. Phys.* **1976**, *32*, 419–442, DOI: 10.1080/00268977600103211.

(63) Flint, C. D.; Tanner, P. A. Luminescence Spectrum of $Cs_2UO_2Cl_4$. *J. Chem. Soc., Faraday Trans. 2* **1978**, *74*, 2210–2217, DOI: 10.1063/1.1731876.

(64) Dau, P.; Su, J.; Liu, H.-T.; Huang, D.-L.; Li, J.; Wang, L.-S. Photoelectron Spectroscopy and the Electronic Structure of the Uranyl Tetrachloride Dianion: $UO_2Cl_4^{2-}$. *J. Chem. Phys.* **2012**, *137*, 064315, DOI: 10.1063/1.4742062.

(65) Matsika, S.; Zhang, Z.; Brozell, S.; Blaudeau, J.-P.; Wang, Q.; Pitzer, R. Electronic Structure and Spectra of Actinyl Ions. *J. Phys. Chem. A* **2001**, *105*, 3825–3828, DOI: 10.1021/jp003085z.

(66) van Besien, E.; Pierloot, K.; Görller-Walrand, C. Electronic Spectra of Uranyl Chloride Complexes in Acetone: A CASSCF/CASPT2 Investigation. *Phys. Chem. Chem. Phys.* **2006**, *8*, 4311–4319, DOI: 10.1039/b607026d.

(67) Pierloot, K.; van Besien, E. Electronic Structure and Spectrum of UO_2^{2+} and $UO_2Cl_4^{2-}$. *J. Chem. Phys.* **2005**, *123*, 204309, DOI: 10.1063/1.2121608.

(68) Wang, Z.; Zachara, J. M.; Liu, C.; Gassman, P. L.; Felmy, A. R.; Clark, S. B. A Cryogenic Fluorescence Spectroscopic Study of Uranyl Carbonate, Phosphate and Oxyhydroxide Minerals. *Radiochim. Acta* **2008**, *96*, 591–598, DOI: 10.1524/ract.2008.1541.

(69) Bernhard, G.; Geipel, G.; Reich, T.; Brendler, V.; Amayri, S.; Nitsche, H. Uranyl(VI) Carbonate Complex Formation: Validation of the $Ca_2UO_2(CO_3)(3)\,(aq\cdot)$ Species. *Radiochim. Acta* **2001**, *89*, 511–518, DOI: 10.1524/ract.2001.89.8.511.

(70) Geipel, G.; Amayri, S.; Bernhard, G. Mixed Complexes of Alkaline Earth Uranyl Carbonates: A Laser-Induced Time-Resolved Fluorescence Spectroscopic Study. *Spectrochim. Acta, Part A* **2008**, *71*, 53 – 58, DOI: 10.1016/j.saa.2007.11.007.

(71) Mori, K.; Goumans, T.; Van Lenthe, E.; Wang, F. Predicting Phosphorescent Lifetimes and Zero-Field Splitting of Organometallic Complexes with Time-Dependent Density Functional Theory Including Spin–Orbit Coupling. *Phys. Chem. Chem. Phys.* **2014**, *16*, 14523–14530, DOI: 10.1039/c3cp55438d.

(72) Parr, R. G.; Pearson, R. G. Absolute Hardness: Companion Parameter to Absolute Electronegativity. *J. Am. Chem. Soc.* **1983**, *105*, 7512–7516, DOI: 10.1021/ja00364a005.

(73) Addleman, R. S.; Wai, C. M. Luminescence Quenching of $UO_2(NO_3)_2 \cdot 2\,TBP$ in Supercritical Fluid CO_2. *Phys. Chem. Chem. Phys.* **1999**, *1*, 783–790, DOI: 10.1039/A807753C.

TOC Graphic

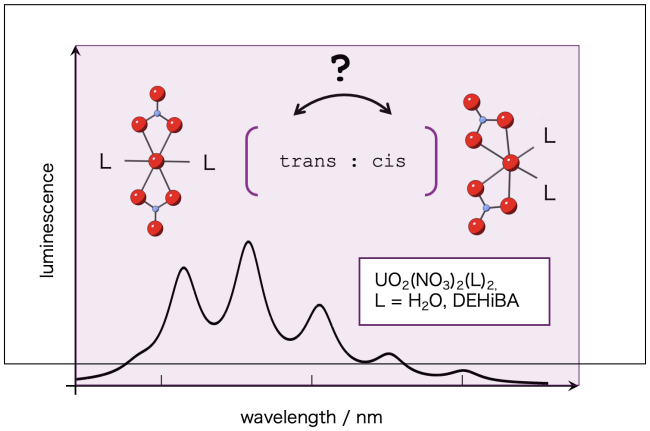

By comparing the available experimental spectra of uranyl complexes and a newly recorded one, in which the latter is in interaction with large organic ligands, with extensive *ab initio* simulations, we rationalize to which extent the inorganic and organic uranyl coordination spheres, as well as the solvent polarity, influence the spectral shapes and vibrational progressions. Relativistic density functional theory (DFT) calculations of the luminescence spectra based on the Franck-Condon principle allow us to reproduce and assign the peak positions.